Superior performance of ablative glass coatings containing graphene nanosheets[1]

Eugenio Garcia, Andres Nistal[2], M. Isabel Osendi, Pilar Miranzo[3]

Institute of Ceramics and Glass (ICV-CSIC), Madrid, Spain

ABSTRACT

Glass with compositions in the Y_2O_3-Al_2O_3-SiO_2 (YAS) system are envisaged as promising high temperature protecting coatings for silicon carbide based composites intended for thermal protection systems (TPS) in aerospace applications. Recently, it has been shown that thermally sprayed YAS hybrid coatings containing a small amount of graphene nanoplateletes (GNPs) developed electrical functionality and higher mechanical compliance as compared to the blank YAS coating. Nevertheless, for TPS, it is crucial to know if they also have a good response under ablation conditions. Hence, the ablative behavior of YAS/GNPs coatings is here addressed using laboratory conditions of high temperature (up to ~ 1350 ºC) and blowing gasses. Results evidence that hybrid coatings, flame sprayed over SiC substrates, with just 1.05 vol.% GNPs show enhanced ablation resistance withstanding up to 30 cycles at 1350 ºC, without signs of spallation or substrate damage, which postulates them as promising TPS candidates. This

[2] Presently at School of Mechanical and Aerospace Engineering, Queen's University, Belfast, UK.
[3] pmiranzo@icv.csic.es

favorable performance seems linked to their strongly direction dependent thermal conductivity, actually becoming in-plane enhanced and through-thickness reduced and thus constraining coating degradation just to the upper-most layer.

KEYWORDS

graphene, glass-ceramics, silicon carbide, coatings, thermal spraying, ablation, thermal conductivity, thermal protection systems

1 Introduction

Carbon and silicon carbide composites reinforced with carbon fibers (C_f/C and C_f/SiC, respectively) have been steadily substituting metals in a variety of applications due to their better thermomechanical performance. Particularly, the use of composites for high temperature heat shielding in aerospace applications has become essential[1-5] in certain areas -as the nose, wings and fin leading edges of sub-orbital Reusable Launch Vehicles- where high reentry temperatures of 900 ⁰C - 1200 ⁰C jointly with mechanical loads develop.[1,2] Although C_f/C and C_f/SiC are the more promising materials for those zones, their rapid degradation in oxidizing atmospheres above 500 ⁰C makes mandatory their protection by means of ablative coatings.[6-9] The major concerns regarding coatings include reducing weight, decreasing vulnerability to orbital debris, while keeping minimal thermal conductivity and high-emissivity to ensure the maximum rejection of incoming convective heat through radiative heat transfer.[4] In that context, we see hybrid

graphene/glass-ceramic coatings as very promising materials, because of the exceptional properties of carbon allotropes as well as the heat resistance and the self-healing capabilities of glass-ceramics.[10,11] The feasibility of the flame spraying method for coating SiC, C_f/SiC and C_f/C substrates using glass (G) and glass-ceramic (GC) compositions of the Y_2O_3-Al_2O_3-SiO_2 (YAS) system has been proved previously by some of the present authors.[12-14] These coatings were continuous, homogeneous, dense and presented good adhesion to SiC, C_f/SiC and C_f/C substrates, particularly for SiC-based material.[14] Furthermore, the inclusion of graphene nanoplatelets (GNPs) as filler for the YAS glass produced anisotropic hybrid coatings with aligned GNPs, exhibiting enhanced damage tolerance and also added electrical and thermal functionalities.[11] Preliminary ablation tests performed in those YAS glass coatings showed endured ablation resistance at 900 ºC, but at higher temperatures the complete removal of the coating occurred.[13] Although promising, these data were far from aimed for thermal protection systems (TPS). Hence, we pretend to increase the thermal resistance of these coating by choosing a YAS composition of higher melting temperature, able to crystallize into a glass-ceramic. Furthermore, the crucial effect that GNP fillers might have on the ablation behavior has not been addressed until now.

In the present work, we evaluate the performance of hybrid glass-ceramic/GNPs coatings, thermal sprayed over SiC substrates, under ablation tests at a maximum temperature of 1350 ºC and also in thermal cycling, comparing with results of corresponding plain coating. The effect of ablation conditions on the coating

microstructure and phases is assessed and, accordingly, an ablation mechanism is proposed for these GNP containing coatings.

2 Experimental

High purity (>99.7%) Y_2O_3 (H.C. Starck,Germany), Al_2O_3 (SM8, Baikowski, France) and SiO_2 (Alfa Aesar, Germany) powders were employed for the selected glass-ceramic (GC) composition $36.0Y_2O_3{:}18.0Al_2O_3{:}46.0SiO_2$ (in mol.%). This composition was conditioned for obtaining spherical shaped particles of ~30 µm following the procedure described elsewhere.[15] Similar size granules for the GC composition with 10 vol. % (6.5 wt %) of graphene nanoplatelets (N008-100-P-10, Angstron Materials Inc., U.S.), labelled as GC/GNPs, were also prepared.[11]

SiC plates (Hexoloy S.A., Saint-Gobain) of 25 x 25 x 4 mm^3 with a density of 3.15 $g{\cdot}cm^3$ were used as substrates, previously sand blasted and flame sprayed with a silicon bond coat for better coating anchoring.[16] GC and GC/GNPs granules were thermally sprayed with an oxyacetylene gun (Casto-Dyn 8000; Eutectic Castolin, Spain), using acetylene and oxygen pressures of $7{\cdot}10^4$ and $4{\cdot}10^5$ Pa, respectively, and gas flow rates of 23.7 and 32.5 in SLPM (standard litres per minute) for each gas; stand-off distance of 14 cm and a powder feed rate fixed at 10 $g{\cdot}min^{-1}$ were standard conditions for all coatings.

The naked-eye inspection revealed the colour difference between the plain GC (white) and the GC/GNPs coatings (black). The density of coatings was measured by the water immersion technique in freestanding coatings obtained by flame

spraying the powders on metallic substrates. As certain vaporization of the nanoplatelets occurred during flame spraying, estimation of the remaining fraction in the coatings was done by thermogravimetric analyses, in a similar way as described in reference 11. The glass transition temperature, the temperature for first crystallization and the melting point of the resulting glass-ceramic GC coating were recorded by differential thermal analysis (DTA-TGA, STA 409 NETZSCH) using a heating rate of 10 K·min^{-1}.

The microstructure of the coatings was observed in fractured specimens, on the top surface and polished cross sections with a table-top Scanning Electron Microscope (SEM, TM1000, Hitachi, Japan). Changes in crystalline phases were followed by X-ray diffraction analyses (XRD, Xpert PRO, PANalytical, Netherlands) performed on the coatings top surface. For a precise observation of how ablation tests affected GNPs, Raman spectra were acquired from polished cross-sections of coatings (original and ablated) using a confocal μ-Raman imaging system (Alpha 300 WITec GmbH, Germany) with a laser excitation wavelength of 532 nm. Raman maps of 150 x 150 pixels (scanning area of 45 μm × 45 μm) and 30 x 200 pixels (25 μm × 125 μm) were acquired, recording one spectrum per pixel and using 60 ms of acquisition time.

Two types of square specimens with different side lengths, 8.8 mm and 20 mm, but same thickness (0.86 mm) were prepared for each coating/Si/SiC system. The approximated thickness of every layer were ~ 0.20 mm for the coating, ~0.06 mm for the Si bond coat and ~0.6 mm for the SiC substrate. These specimens were used to measure the in-plane ($\alpha_{in-plane}$) - square of 20 mm side - and through-

thickness ($\alpha_{thickness}$) - 8.8 mm square - apparent thermal diffusivities at room temperature by the laser-flash method (Thermaflash 2200, Holometrix/Netzsch, ~~U.S.~~). The thermal conductivity of the GC and GC/GNPs coatings ($\kappa_{thickness}$) was calculated using analytical models for heat diffusion in layered systems[17] and iterative software routines, using the $\alpha_{thickness}$ data of the corresponding systems and referred values for thermal properties of SiC and Si.[16] The specific heat (C_p) was estimated by the rule of mixtures using thermodynamic data.[18]

A special set-up was utilized for the apparent $\alpha_{in-plane}$ of the systems, consisting of two masks, one to confine the laser pulse on the center of the specimen surface, into a circle of $r_0 = 2.5$ mm radius, and another to define an annulus of radius $r = 2.2r_0$ on the opposite surface facing the IR detector. The recorded temperature rise due to the radial heat flow is fitted by a two-dimensional model.[19] Diffusivity data were averaged over at least 5 measurements.

Ablative and cycling tests were performed by focusing the oxyacetylene flame on the coating surface at a stand-off distance of 9 cm, using the same conditions above described but adjusting the gas flow (see details in Table I) to achieve the target temperatures, namely 900 and 1200°C for ablation and 1350 °C for thermal cycling. The surface temperature of the exposed specimen (coating face) was continuously recorded during ablation tests by an IR pyrometer (IMPAC IGAR 12-LO, LumaSense Tech., US) focussed on the coating surface. The temperature of the back side of the SiC substrate was logged by a thermocouple attached to it and protected from the flame. The thermal exposure was cut-off after 30s of holding at the set point temperature. The cycling tests were done by focusing successively

the flame over the coating -until the temperature of 1350 °C was reached- and then blowing air onto the specimen -at 3 bars of pressure- to rapidly cool down the surface, typically at 200 °C in ~ 30 s. Each heating-cooling cycle was repeated 30 times in two different samples.

3 Results and discussion

The cross sections of the GC and GC/GNPs sprayed coatings are shown in Fig. 1, where perfect attachment between the different layers is perceived. Both coatings are dense, continuous and have a thickness of ~ 130 μm. Plain CG coating is formed by splats (see insert in Fig. 1a) of different grey contrast, produced by local variations of composition, and contains some disperse pores. On the other hand, the elongated features observed at the splat boundaries in the GC/GNPs coating (Fig. 1b) correspond to the nanoplatelets.[11] As the DTA of the GC ground coating (Fig. 2a) shows, temperatures of glass transition (T_g), first crystallization (T_c) and melting (T_m) are 929, 1055 and 1525 °C, respectively. Therefore, present GC coating melts at a temperature ~ 100 °C above that registered for the previously formulated coating, G glass[13] (T_m = 1418 °C) of composition $19.2Y_2O_3:32.4Al_2O_3:48.4SiO_2$ (in mol%); besides, GC coating shows a narrower viscous flow window (~126 °C) than that shown by G coating (200°C) of higher $Al_2O_3:Y_2O_3$ ratio (1.7 versus 0.5 of GC).[20] Therefore, the present GC coating is expected to show improved thermal resistance and satisfactory self-healing ability.

The remaining GNPs in the GC hybrid coating, as determined by TGA, amount to 1.05 vol.%, representing 16 % of the initial content. Surprisingly, this percentage is

noticeably lower than that previously obtained for the G hybrid coating with 3.54 vol % of lasting GNPs.[11] The lower amount of surviving GNPs for the GC coating may be explained by both its higher melting temperature and the lower amount of energy absorbed by the GC feedstock granules during spraying for reacting and melting, compared to the G feedstock; as seen in Fig. 2b. Hence, the total energy consumption estimated by integrating the area of DTA bands for the G and GC feedstock, from the first reaction event up to the melting (1430 and 1525ºC, respectively), gave 11 $\mu V \cdot s \cdot mg^{-1}$ for G and 2 $\mu V \cdot s \cdot mg^{-1}$ for GC. In this way, during spraying, there would be a higher amount of heat available in the flame for GNPs damaging, up to higher temperatures and for longer times, in the case of GC granules. This finding appears decisive when designing new glass-ceramic/GNPs compositions for thermal spraying processing.

The ablation test set-points of 900 ºC and 1200 ºC are reached on both coatings after 50 and 20 s, respectively; the faster rate for the 1200 ºC test owing to the higher power flame used (Table I). During the 30 s of thermal exposure, the surface coating temperature monotonically rose until the top values of 949°C (GC/GNP) and 962°C (GC) for the 900 ºC treatment, whereas 1352°C (GC/GNP) and 1459°C (GC) were registered for the 1200 ºC ablation test (as an example, heating curves of the 1200 ºC test are depicted in Fig. 3a). Hence, temperatures in the hybrid coating are comparatively lower than in the corresponding plain coating for both set conditions, and the same is observed for the back side temperatures of the SiC substrates, which could be explained by the higher emissivity –as the hybrid coatings are black- and anisotropic thermal conductivity of the GNP

containing coatings. As seen in Table II, $\alpha_{in-plane}$ of the GC/GNPs system increases by ~8% (from 3.43 to 3.71 $\times$ 10^{-5} m^2·s^{-1}) despite the existence in the coating of just ~1 vol.% GNPs, whereas the $\alpha_{thickness}$ is reduced by 38% (from 0.93 to 0.58 $\times$ 10^{-5} m^2·s^{-1}). Furthermore, the $\kappa_{thickness}$ calculated for the GC/GNPs coating (0.31 W·m^{-1}·K^{-1}) is~ 27% lower than the value obtained for the GC coating (0.43 W·m^{-1}·K^{-1}). This anisotropic behavior is similar to that observed in bulk ceramic materials having oriented GNPs lying in a perpendicular direction to the heat flux,[21] being the reduction for the cross-plane thermal conductivity mainly related to the intrinsically lower conductivity of the graphite in the c direction. However, it differs from the thermal performance previously reported for the G glass coating containing 3.6 vol.% GNPs; in that case, an augment of κ by 30 % was measured for both orientations because GNPs were also connected in the direction perpendicular to the coating surface.[11] For the present coatings, the reduced amount of GNPs intensifies the thermal anisotropy of the hybrid GC/GNP coating (the $\alpha_{in-plane}/\alpha_{thickness}$ ratio rises from 3.7 to 6.4), which foresees good performance for thermal shield purposes, as they would enhance the in-plane release of heat avoiding hot spots while hindering heat propagation towards the substrate in the through-thickness direction. Furthermore, the higher emissivity of GC/GNPs compare to GC favours rejection of incoming convective heat through radiative heat transfer.

The formation of blisters was noticed on the GC coating surface, probably caused by the simultaneous action of the blowing gases and the reduction of glass viscosity due to the increasing temperatures, in a similar way to which G

composition tested at 900 °C behaved.[13] However, the GC coating develops significantly smaller size bubbles because of its comparatively higher Tg and narrower viscous flow window (Fig. 2). Besides, the GC coating survived the 1200 °C ablation test without spalling. Therefore, the new GC coating has better thermal resistance than the G one, which was entirely removed above 900 °C.[13] On the other hand, bubbles are hardly detected in the GC/GNPs coating tested at 900 °C and 1200 °C as it would have higher viscosity associated to both the lower temperature reached during the tests (Fig. 3b) and the presence of GNPs. These coatings turned their original black colour into white, suggesting the GNPs burning close to the surface.

The improved resistance to ablation caused by the GNPs is quite evident from the coatings cross section images of Fig. 4. The GC/GNPs coating tested at 900 °C (Fig. 4c) seems hardly affected whereas the plain GC coating (Fig. 4a) shows some thickness reduction (26 μm) and bubbles formation on the surface. At 1200°C, the plain GC coating (Fig. 4b) reveals extended cavitation next to the Si bond coat, generated by the expansion of dissolved gases that cannot escape. This harsh damage is not observed in the GC/GNPs coating (Fig. 4d), according to the lower temperatures achieved and the reported gas barrier properties of graphene;[22] hence, GNPs may limit the penetration of combustion gasses considering that they form an almost continuous layer.

The distribution of GNPs across the GC/GNPs hybrid coatings before and after ablation tests was evaluated on the coating cross-section by Raman spectroscopy (Fig 5). The mapping built by filtering the I_G Raman band characteristic of the

graphitic structures[23] on an area of 25 μm x 125 μm reveals a network of GNPs along the entire as-sprayed coating (Fig. 5a), whereas after ablation at 1200 ºC (Fig. 5b), GNPs dissapear in a degraded top layer of ~45 μm, remaining unaltered in the inner area of the coating cross section. The I_D/I_G ratio calculated for the window averaged spectra recorded in the central area of the coatings were very similar (0.40-0.43) for the as-sprayed and ablated coating (Fig. 5c,d), thus proving the low degradation of the inner GNPs during ablation despite reaching surface temperatures of 1390 ºC. These I_D/I_G values were always higher than that of the original GNPs[11] probably because of the higher contribution of the defective GNP edges when analyzing the coating cross-section. The confinement of GNPs degradation at the uppermost surface proves that the interaction with the hot gasses is restrained to a certain depth, slowing the degradation underneath, and consequently providing the hybrid coating with a higher thermal load resistance under ablation conditions. The thickness of the degraded layer for each coating as function of the maximum temperature reached during the ablation test is shown in Fig. 3b. This thickness is significantly lower in the case of the GC/GNPs coating for both ablation temperatures which confirms again the GNPs positive effect.

As seen in Fig. 6, the XRD patterns of the as-sprayed coatings display the characteristic amorphous bump, with a superimposed diffraction peak at 26° associated to the (003) graphite reflection in the case of the hybrid coating. Therefore, they were essentially amorphous, which must be connected to the fast cooling rates of the molten droplets after impinging on the substrate (~10^8 – 10^9 K·s^{-1})[24] as the GC composition is outside of the glass forming region of the Y_2O_3-

Al_2O_3-SiO_2 phase equilibrium diagram.[25-27] After ablation at 900 ºC, an extensive crystallization is not observed, particularly for the GC/GNPs coating that still exhibits a marked amorphous halo, inferring that GNPs hindered crystallization probably because of the lower achieved temperature. Crystallization augmented in both coatings after ablation at 1200 ºC, as reached temperatures were well above the first crystallization temperature of the GC composition (1055 ºC, see Fig. 2a), showing diffraction peaks of yttrium silicates (YAG and O-apatite $Y_{4.67}(SiO_4)_3O$) and aluminum yttrium oxide phases ($Al_2Y_4O_9$), which do not correspond to those predicted by the corresponding equilibrium phase diagram[28] (YAG, Y_2SiO_5 and $Y_2Si_2O_7$). This crystallization has been also proved by Raman point spectra recorded on individual splats ("O" in Fig. 4a,b) that showed just the band at ~950 cm^{-1} ascribed to aluminosilicate glasses[29] in the as-sprayed GC/GNPs coating but some additional bands associated to crystalline phases for the same coating ablated at 1200 ºC; this fact reveals that temperatures above the Tg of GC (1055 ºC) were achieved inside coating during ablation.

The high temperature stability and performance of the GC/GNPs coating was further proved by thermal cycling tests (Table I), where no-spallation signs were detected after 30 cycles at 1350 ºC. Observation of the coating cross section (Fig. 7a) shows voids formation across the coating although it still remains perfectly attached to the Si bond coat, without any indication of damage along the coating/bond-coat and bond-coat/substrate interfaces. The XRD pattern of the top surface after cycling (Fig. 7b) showed crystallization of yttrium mono- and di-silicates together with YAG as the main phases, in agreement with the Y_2O_3-Al_2O_3-

SiO_2 phase equilibrium diagram predictions.[28] Therefore, the hybrid GC/GNPs coating successfully accomplished the goal of harsh thermal protection at 1350°C. Moreover, this type of ablative coatings could be re-sprayed, after removal of the damaged coating, then allowing convenient in-situ restoring.

4 Conclusions

Thick glass-ceramic/multilayer graphene hybrid coatings flame sprayed on SiC substrates from granules of Y_2O_3-Al_2O_3-SiO_2 powders and graphene nanoplatelets are visualized as promising candidates for TPS. With just 1 vol.% of GNPs, the hybrid coating shows enhanced ablation resistance as compared to the blank coating, in fact protecting the substrate from harsh exposures at 1350 °C for at least 30 s. They also resist up to 30 cycles at a 1350 °C without spallation or substrate damage. This enhanced ablation resistance is linked to the higher emissivity and improved anisotropy in thermal conductivity of the hybrid coating which limits hot spots generation while hinder heat propagation towards the substrate. The ablation confines GNPs degradation just at the uppermost layer because the horizontally arranged GNP network limits the interaction of the hot gasses with the underneath coating, consequently providing the hybrid coating with a higher thermal load resistance.

References

1. D. E. Glass, "Ceramic matrix composite (CMC) thermal protection systems (TPS) and hot structures for hypersonic vehicles"; pp. 1−36 in *15th AIAA*

space planes and hypersonic systems and technologies conference. Dayton, Ohio, 2008.

2. B. Behrens and M. Muller, "Technologies for Thermal Protection Systems Applied on Re-usable Launcher", *Acta Astronaut.*, **55** [3] 529-536 (2004).

3. P. Sanoj and B. Kandasubramanian, "Hybrid Carbon-Carbon Ablative Composites for Thermal Protection in Aerospace" *J. Compos.*, **2014** 825607 15pp. (2014)

4. J. Young and R. Crippen, "Thermal Protection Systems"; pp 182−199 in Vol. 3409, *Wings in Orbit: Scientific and Engineering Legacies of the Space Shuttle, 1971− 2010*. Edited by W. Hale et al. Government Printing Office, Washington DC, 2011.

5. W. Krenkel and F. Berndt, "C/C−SiC Composites for Space Applications and Advanced Friction Systems," *Mater. Sci. Eng. A,* **412** [1] 177−181 (2005).

6. J.E. Sheehan, K.W. Buesking and B.J. Sullivan, "Carbon-Carbon Composites," *Annu. Rev. Mater. Sci.*, **24** [1] 19−44 (1994).

7. I. Spitsberg and J. Steibel, "Thermal and Environmental Barrier Coatings for SiC/SiC CMCs in Aircraft Engine Applications," *Int. J. Appl. Ceram. Technol.*, **1** [4] 291−301 (2004).

8. L. He-Jun, X. Hui, F. Qian-Gang, Z. Yu-Lei, S. Xiao-Hong, and L. Ke-Zhi, "Research Status and Prospect of Anti-Oxidation Coatings for Carbon/Carbon Composites," *J. Inorg. Mater.*, **25** [4] 337−343 (2010).

9. I. Sakraker and C.O. Asma, "Experimental Investigation of Passive/Active Oxidation Behavior of SiC Based Ceramic Thermal Protection Materials Exposed to High Enthalpy Plasma," *J. Eur. Ceram. Soc.*, **33** [2] 351−359 (2013).

10. F. Smeacetto, M. Ferraris and M. Salvo, "Multilayer Coating with Self-sealing Properties for Carbon-Carbon Composites," *Carbon*, **41** [11] 2105−2111 (2003).

11. E. Garcia, A. Nistal, A. Khalifa, Y. Essa, F. Martín de la Escalera, M. I. Osendi and P. Miranzo, "Highly Electrically Conducting Glass-Graphene Nanoplatelets Hybrid Coatings," *ACS Appl. Mater. Interfaces*, **7** [32] 17656−17662 (2015).

12. M.A. Sainz, M.I. Osendi and P. Miranzo, "Protective Si-Al-O-Y Glass Coatings on Stainless Steel in Situ Prepared by Combustion Flame Spraying," *Surf. Coat. Technol.*, **202** [9]1712−1717 (2008).

13. E. García, A. Nistal; F. Martín de la Escalera, A. Khalifa, M.A. Sainz, M.I. Osendi and P. Miranzo, "Thermally Sprayed Y_2O_3-Al_2O_3-SiO_2 Coatings for High Temperature Protection of SiC Ceramics," *J. Therm. Spray Technol.*, **24** [1-2] 185−193 (2015).

14. C. Marraco-Borderas, A. Nistal, E. García, M. A. Sainz, F. Martín de la Escalera, Y. Essa and P. Miranzo, "Adhesion of Y_2O_3-Al_2O_3-SiO_2 coatings to typical aerospace substrates," (Spanish). *Bol. Soc. Ceram. V.* In-press (2016).

15. E. García, J. Mesquita-Guimarães, P. Miranzo and M.I. Osendi, "Porous Mullite and Mullite-ZrO_2 Granules for Thermal Spraying Applications," *Surf. Coat. Technol.*, **205** [17] 4304−4311 (2011).

16. A. Nistal, E. García, C. García-Diego, M.I. Osendi and P. Miranzo, "Flame Spraying of Adherent Si Coatings on SiC Substrates," *Surf. Coat. Technol.*, **270** 8−15 (2015).

17. T. Y. R. Lee, "Thermal Diffusivity of Dispersed and Layered Composites"; Ph.D. Thesis, Purdue University, West Lafeyette, IN, 1977.

18. A. Roine, "Outokumpu HSC Chemistry for Windows, version 5.11"; Outokumpu Research: Pori, Finland, 2002.

19. A. B. Donaldson and R.E. Taylor, "Thermal Diffusivity Measurement by a Radial Heat Flow Method," *J. Appl. Phys.*, **46** [10] 4584−4589 (1975).

20. L. Wu, G. Liu, J. Li, B. He, Z. Yang and Y. Chen, "Dependence of Glass-Forming Ability on Starting Compositions in Y_2O_3- Al_2O_3-SiO_2 System," *Ceram-Silikaty*, **55** [3] 228−231 (2011).

21. P. Miranzo, E. García, C. Ramírez, J. González-Julián, M. Belmonte and M.I. Osendi, "Anisotropic Thermal Conductivity of Silicon Nitride Ceramics Containing Carbon Nanostructures," *J. Eur. Ceram. Soc.*, **32** [8] 1847−1854 (2012)

22. J.S. Bunch, S.S. Verbridge, J. S. Alden, A. M. van der Zande, J.M. Parpia, H. G. Craighead and P.L. McEuen, "Impermeable Atomic Membranes from Graphene Sheets," *Nano Lett.*, **8** [8] 2458−2462 (2008).

23. A. C. Ferrari, J.C Meyer, V. Scardaci, C. Casiraghi, M. Lazzeri, M. F. Mauri, S. Piscanec, D. Jiang, K.S. Novoselov, S. Roth and A.K. Geim, "Raman Spectrum of Graphene and Graphene Layers," *Phys. Rev. Lett.*, **97** [18] 187401−187404 (2006).

24. L. Bianchi, A.C. Leger, M. Vardelle, A. Vardelle, and P. Fauchais, "Splat Formation and Cooling of Plasma-Sprayed Zirconia," *Thin Solid Films*, **305** [1] 35−47 (1997).

25. M.J. Hyatt and D.E. Day, "Glass Properties in the Yttria-Alumina-Silica System," *J. Am. Ceram. Soc.*, **70** [10] C283−C287 (1987).

26. J.E. Shelby, S.M. Minton, C.E. Lord and M.R. Tuzzolo, "Formation and Properties of Yttrium Aluminosilicate Glasses," *Phys. Chem. Glasses*, **33** [3] 93−98 (1992).

27. K. Morita, A. Umezawa, S. Yamato, and A. Makishima, "Surface-Roughness of Yttria-Containing Aluminosilicate Glass-Ceramics as Indicative of Their Machinability," *J. Am. Ceram. Soc.*, **76** [7] 1861−1864 (1993).

28. U. Kolitsch, H.J. Seifert, T. Ludwig, and F. Aldinger, "Phase Equilbria and Crystal Chemistry in the Y_2O_3-Al_2O_3-SiO_2 System," *J. Mater. Res.*, **14** [2] 447−455 (1999).

29. J. T. Kohli,R.A. Condrate, J.R. Shelby, "Raman and Infrared Spectra of Rare Earth Aluminosilicate Glasses," *Phys. Chem. Glasses*, **34** [3] 81−87 (1993).

Captions

Figure 1. SEM images of the polished cross-sections of (a) GC and (b) GC/GNPs coatings. The inserts show higher magnification details of the coatings.

Figure 2. DTA curves of the plain GC and G compositions for (a) the coatings indicating the temperatures for glass transition (T_g), first crystallization event (T_c) and melting (T_m); and (b) the original feedstock powders where grey areas show the exothermic and endothermic events integrated for the calculation of the energy consumed for the reacting and melting processes during spraying.

Figure 3. (a) Temperatures measured at the front surface of the GC and GC/GNPs coatings and the back surface of the SiC substrate versus ablation time during the tests at 1200 ºC. (b) Thickness of the degraded top layer vs. the maximum temperature reached during ablation tests at 900 and 1200 ºC.

Figure 4. SEM micrographs of the cross sections of the GC and GC/GNPs coatings after 900 (a,c) and 1200 ºC (b,d) ablation tests.

Figure 5. Raman studies done on the GC/GNPs hybrid coating: (a) as-sprayed and (b) after the ablation test at 1200 ºC, including optical images of the analysed region and Raman maps of the intensity of the G-band of GNPs acquired on the red boxed region. Representative Raman spectra of as-sprayed (c) and (d) ablated coating corresponding to point analyses of GNPs (X) and GC splats (O) and an average spectrum recorded in an area of 45 µm x 45 µm of the central part of the coatings.

Figure 6. XRD patterns of the surface of the GC and GC/GNPs coatings (as-sprayed and ablated at 900 and 1200 ⁰C), showing evolution of crystalline phases with the ablation temperature.

Figure 7. SEM micrograph of the GC/GNPs coating cross-section (a) and XRD pattern of the top surface (b) after 30 cycles at 1350 ⁰C.

Table I. Flow of gases employed in the different high temperature tests.

	Ablation at 900 ºC	Ablation at 1200 ºC	Cycling at 1350 ºC
O_2 (SLPM)	16.3	18.8	21.5
C_2H_2 (SLPM)	12.0	13.8	13.8

*SLPM: Standard Litres per Minute

Table II. Values of apparent in-plane ($\alpha_{in-plane}$) and through-thickness ($\alpha_{thickness}$) thermal diffusivity measured for the coating/Si/SiC systems. Through-thickness thermal conductivity ($\kappa_{thickness}$) values calculated for the coatings using multilayer models are also shown.

	$\alpha_{in-plane}$ (m^2·s^{-1}) (x10^{-5})	$\alpha_{thickness}$ (m^2·s^{-1}) (x10^{-5})	$\kappa_{thickness}$ (W·m^{-1}·K^{-1})
	coating/Si/SiC		coating
GC	3.43	0.93	0.43
GC/GNPs	3.71	0.58	0.31

Statistical deviations were 10%, 5% and 7% for $\alpha_{in-plane}$, $\alpha_{thickness}$ and $\kappa_{thickness}$, respectively.

Figures paper Superior performance of ablative glass coatings containing graphene nanosheets

Figure 1. SEM images of the polished cross-sections of (a) GC and (b) GC/GNPs coatings. The inserts show higher magnification details of the coatings.
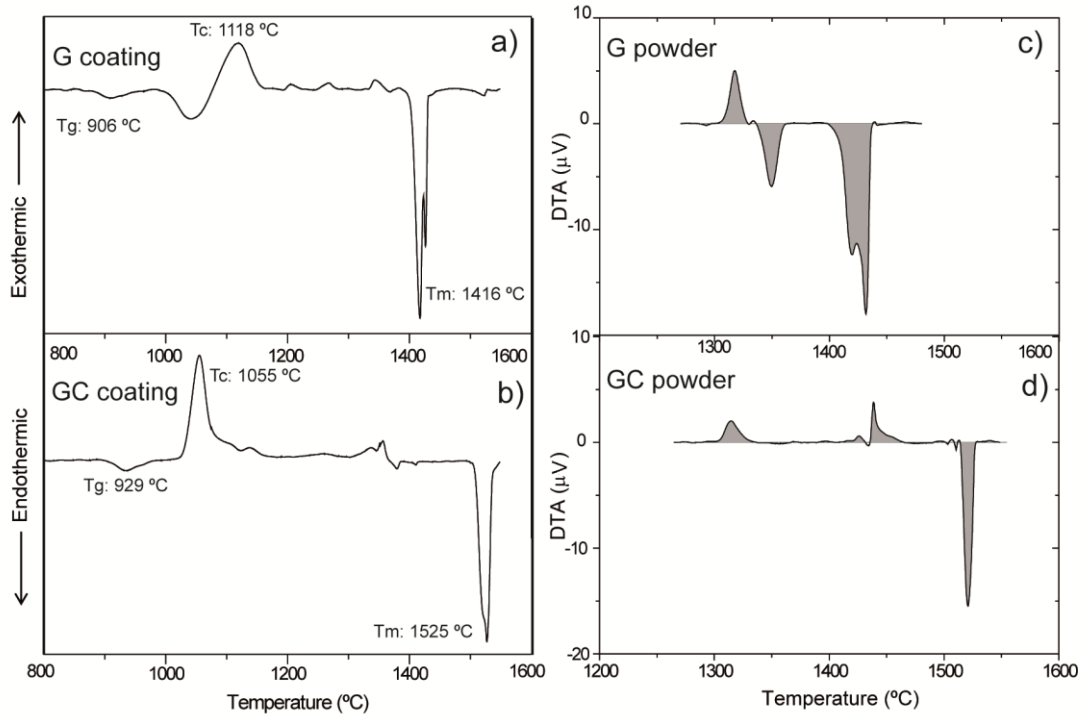
Figure 2. DTA curves of the plain GC and G compositions for (a) the coatings indicating the temperatures for glass transition (T_g), first crystallization event (T_c) and melting (T_m); and (b) the original feedstock powders where grey areas show the exothermic and endothermic events integrated for the calculation of the energy consumed for the reacting and melting processes during spraying.

Figure 3. (a) Temperatures measured at the front surface of the GC and GC/GNPs coatings and the back surface of the SiC substrate versus ablation time during the tests at 1200 ºC. (b) Thickness of the degraded top layer vs. the maximum temperature reached during ablation tests at 900 and 1200 ºC.
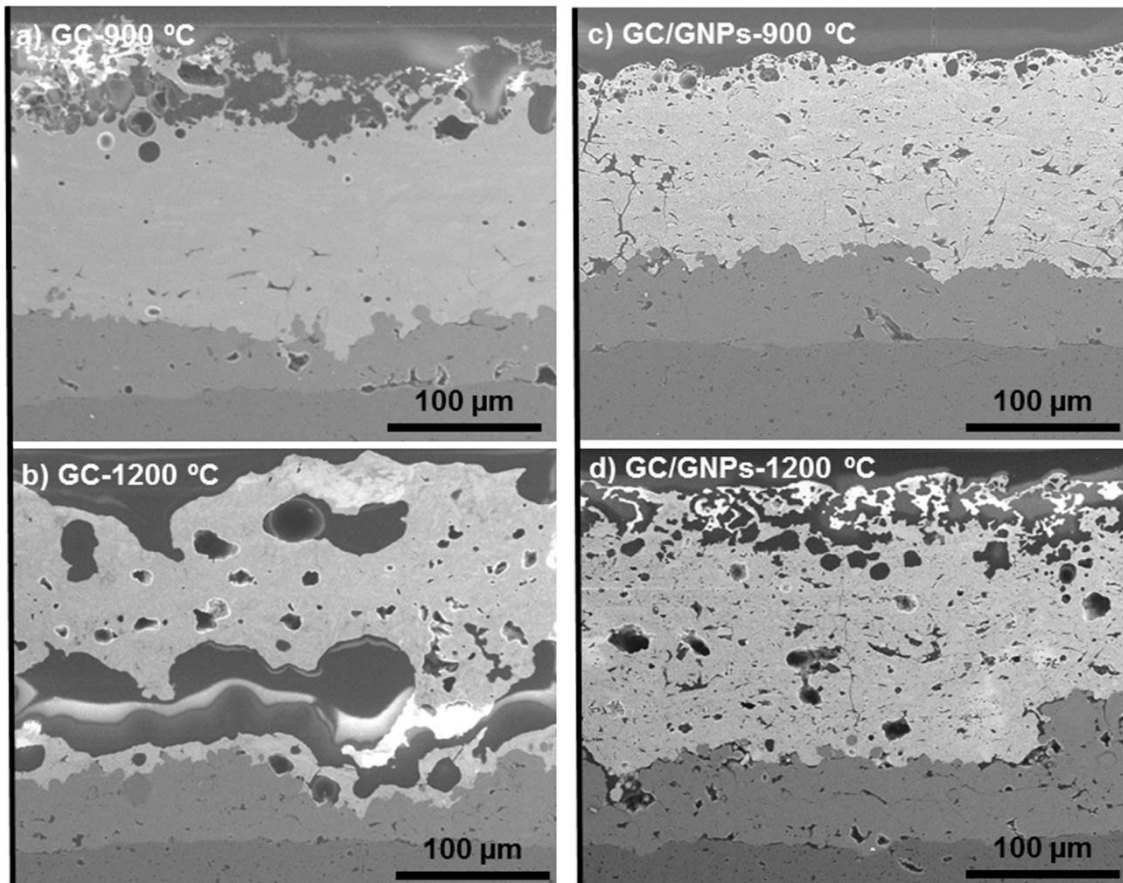
Figure 4. SEM micrographs of the cross sections of the GC and GC/GNPs coatings after 900 (a,c) and 1200 ºC (b,d) ablation tests.
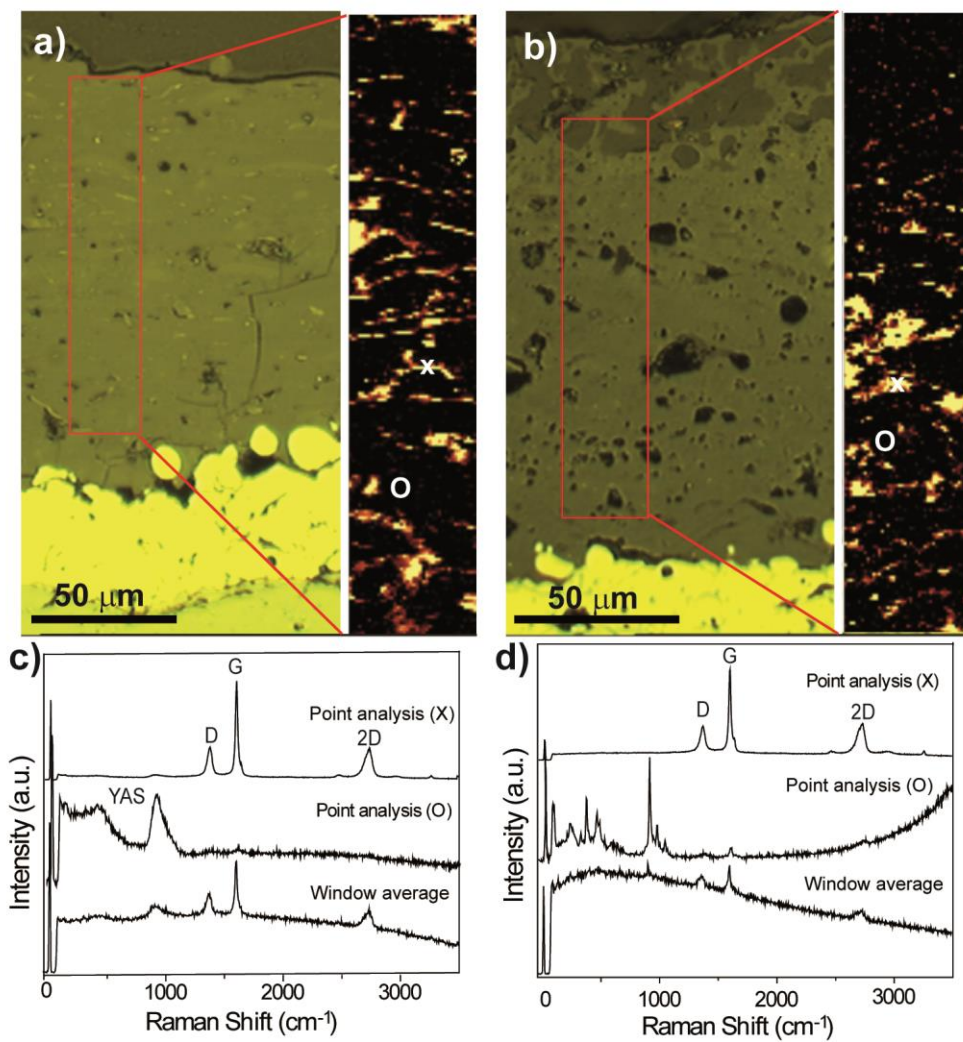
Figure 5. Raman studies done on the GC/GNPs hybrid coating: (a) as-sprayed and (b) after the ablation test at 1200 ºC, including optical images of the analysed region and Raman maps of the intensity of the G-band of GNPs acquired on the red boxed region. Representative Raman spectra of as-sprayed (c) and (d) ablated coating corresponding to point analyses of GNPs (X) and GC splats (O) and an average spectrum recorded in an area of 45 μm x 45 μm of the central part of the coatings.
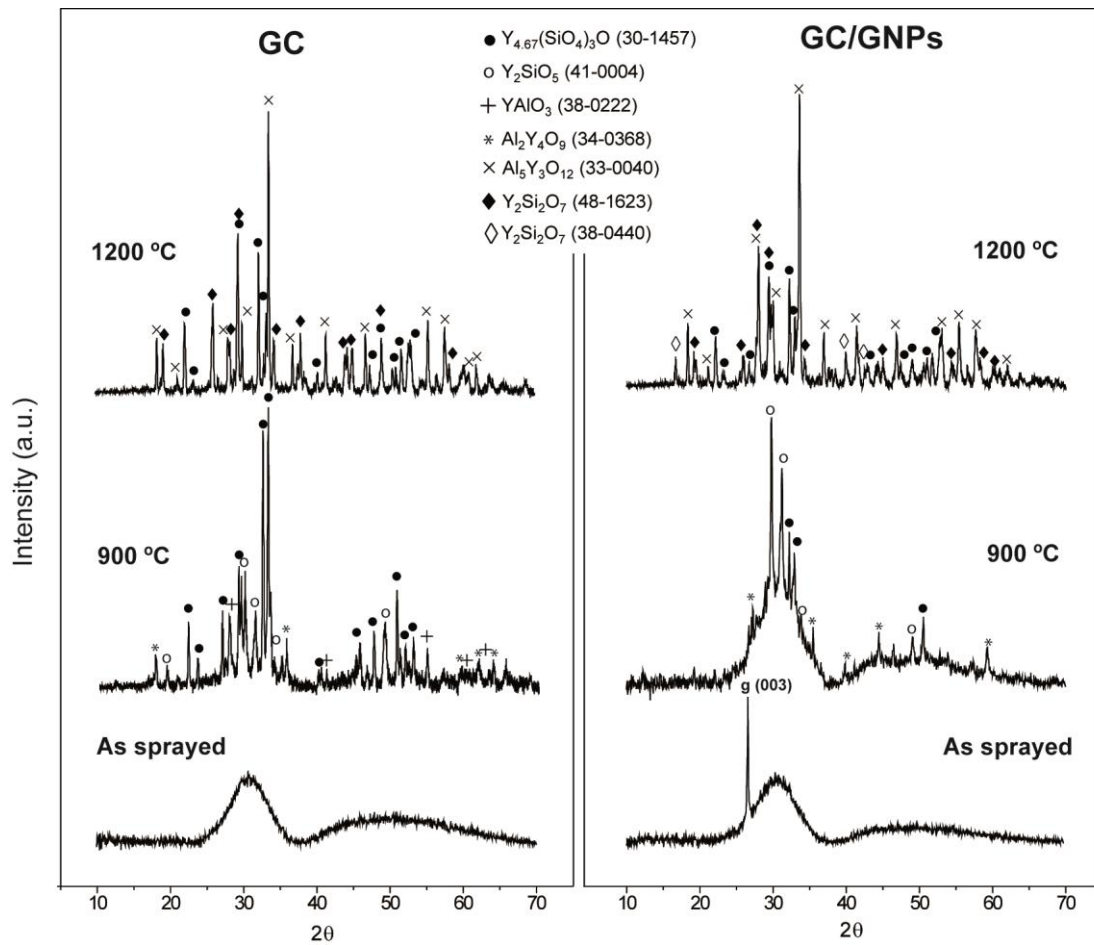
Figure 6. XRD patterns of the surface of the GC and GC/GNPs coatings (as-sprayed and ablated at 900 and 1200 ºC), showing evolution of crystalline phases with the ablation temperature.
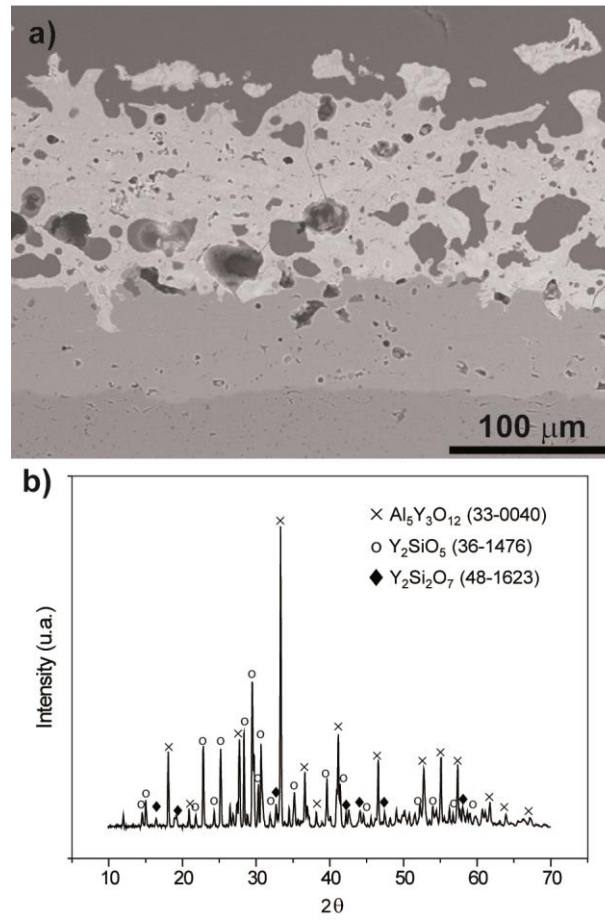
Figure 7. SEM micrograph of the GC/GNPs coating cross-section (a) and XRD pattern of the top surface (b) after 30 cycles at 1350 ºC.